Weierstraß-Institut
für Angewandte Analysis und Stochastik

Leibniz-Institut im Forschungsverbund Berlin e. V.

Preprint ISSN 2198-5855

Micro- and nano-scale engineering and structures shape architecture at nucleation from In-As-Sb-P composition liquid phase on an InAs(100) surface

Karen M. Gambaryan[1], Oliver Marquardt[2], Torsten Boeck[3], Achim Trampert[4]

submitted: October 12, 2020

[1] Dept. of Physics of Semiconductors and Microelectronics
Yerevan State University
1 A. Manoukian Str.
Yerevan 0025
Armenia
E-Mail: kgambaryan@ysu.am

[2] Weierstrass Institute
Mohrenstr. 39
10117 Berlin
Germany
E-Mail: oliver.marquardt@wias-berlin.de

[3] Leibniz Institute for Crystal Growth
Max-Born-Str. 2
12489 Berlin
Germany
E-Mail: torsten.boeck@ikz-berlin.de

[4] Paul Drude Institute for Solid State Electronics
Hausvogteiplatz 5 – 7
10117 Berlin
Germany
E-Mail: trampert@pdi-berlin.de

No. 2775
Berlin 2020

2010 *Physics and Astronomy Classification Scheme.* 73.21.La, 73.22.Dj, 81.10.Dn.

Key words and phrases. Nanostructures, nanoarchitecture, liquid phase epitaxy, electronic properties, infrared photodetectors.

K.M.G acknowledges funding by the Deutscher Akademischer Austauschdienst (DAAD, German Academic Exchange Service) (Personal ref. no.: 91567213) and State Committee of Science of RA for financial support under grant 18T-2J016. O.M. was funded by the Deutsche Forschungsgemeinschaft (DFG, German Research Foundation) under Germany's Excellence Strategy - EXC2046: MATH+ Berlin Mathematics Research Center (project AA2-5).

Edited by
Weierstraß-Institut für Angewandte Analysis und Stochastik (WIAS)
Leibniz-Institut im Forschungsverbund Berlin e. V.
Mohrenstraße 39
10117 Berlin
Germany

Fax: +49 30 20372-303
E-Mail: preprint@wias-berlin.de
World Wide Web: http://www.wias-berlin.de/

Micro- and nano-scale engineering and structures shape architecture at nucleation from In-As-Sb-P composition liquid phase on an InAs(100) surface

Karen M. Gambaryan, Oliver Marquardt, Torsten Boeck, Achim Trampert

Abstract

In this review paper we present results of the growth, characterization and electronic properties of In(As,Sb,P) composition strain-induced micro- and nanostructures. Nucleation is performed from In-As-Sb-P quaternary composition liquid phase in Stranski-Krastanow growth mode using steady-state liquid phase epitaxy. Growth features and the shape transformation of pyramidal islands, lens-shape and ellipsoidal type-II quantum dots (QDs), quantum rings and QD-molecules are under consideration. It is shown that the application of a quaternary In(As,Sb,P) composition wetting layer allows not only more flexible control of lattice-mismatch between the wetting layer and an InAs(100) substrate, but also opens up new possibilities for nanoscale engineering and nanoarchitecture of several types of nanostructures. HR-SEM, AFM, TEM and STM are used for nanostructure characterization. Optoelectronic properties of the grown structures are investigated by FTIR and photoresponse spectra measurements. Using an eight-band $\mathbf{k} \cdot \mathbf{p}$ model taking strain and built-in electrostatic potentials into account, the electronic properties of a wide range of $InAs_{1-x-y}Sb_xP_y$ QDs and QD-molecules are computed. Two types of QDs mid-infrared photodetectors are fabricated and investigated. It is shown that the incorporation of QDs allows to improve some output device characteristics, in particularly sensitivity, and to broaden the spectral range.

1 Introduction

Increasing interest towards semiconductor nanostructures is in the first place caused by the existence of a wide spectrum of possibilities for controlling the properties of semiconducting materials and devices. In quantum dots (QDs), a limitation of the motion of free carriers in all three directions, leading to size-quantization effects, opens an additional possibility of effective control of properties of nanostructure-based devices by means of varying their sizes [6]. The modified density of states in QDs, nanowires, QD-molecules and other nanostructures facilitates an essential improvement of operational optoelectronic parameters of semiconductor devices, such as lasers, photodetectors, or light emitters. In particular, employing QDs in semiconductor lasers leads to a rise in the temperature stability of their parameters, a decrease of threshold currents, broadening of the photodetectors' photosensitivity spectrum and its shift towards the long-wavelength spectral range, enhancement of the efficiency of solar cells [5, 34, 3], and so on. From the point of view of fundamental physics and technology, such phenomena as interactions in coupled QDs [36] and in QD-nanoleaves cooperative structures [28, 14, 2] and influence of QDs on current-voltage and optoelectronic characteristics of device structures have been studied [23, 13]. Among quantum dots and wires fabrication techniques, the self-organized Stranski-Krastanow (S-K) growth mode [38] is an important one by which dislocation-free dots, elongated islands and wires can be produced. By this method, when the islands are in

DOI 10.20347/WIAS.PREPRINT.2775 Berlin 2020

minimum size, QDs exhibit a circular shape. Indeed, above a certain critical thickness, the growth mode switches from the conventional layer-by-layer (i.e. two-dimensional, 2D) to a 3D growth mode due to the accumulation of elastic energy in the strained layer that, first, partially relaxes by spontaneously nucleating small islands of strained material and, later, by creating misfit dislocations. When depositing heteroepitaxial layers, there is a relatively limited amount of materials combinations that can be grown with closely lattice matched parameters. By combining lattice-mismatched layers, the range of available materials combinations may be increased, at the cost of incorporating strain into the grown materials. The lattice mismatch in this case is commonly a few percent compressively strained. For example, at the epitaxy of InAs on GaAs, Ge or SiGe alloy on Si substrate, etc. A layer, which in a 2D fashion, undergoes a phase transition towards 3D growth as the accommodation of elastic strain in a pseudomorphic layer changes the balance between the surface and interface free energies during growth. This results in the formation of coherent (dislocation-free) islands or QDs on the top of a thin wetting layer. Depending on the value of strain, the thickness of the wetting layer varies from a few monoatomic layers until few tens of nanometers. Note, as a curiosity, that in the original publication by Stranski and Krastanow [38], no strain effects were considered. Narrow band-gap III-V semiconductor materials as InAs, GaSb, InSb and their alloys are particularly interesting and useful since they are potentially promising to access mid- and far infrared wavelength regions and should provide the next generation of LEDs, lasers and photodetectors for applications such as infrared gas sensors, molecular spectroscopy, thermal imaging and thermophotovoltaic cells [12]. For mid-IR applications (2-5 μm), QDs are normally formed with binary compounds InAs and InSb or In(As,Sb), (In,Ga)As, (In,Al)As, In(As,P), In(As,Sb,P) etc. alloys, with InP, GaAs, GaSb and InAs used as substrates. Obviously, the key parameters of nanostructures are the shape, size distribution, strain, and chemical composition, which modify the electronic and optical properties of the final product employed in a semiconductor device. Therefore, precise control of the growth process is required in order to produce highly regular mono-disperse QDs arrays. However, many aspects of especially III-V ternary and quaternary compound QDs formation and evaluation and other scientific and technological problems are still poorly understood. There is a well-developed understanding of island nucleation [8, 39] and subsequent coarsening [44] for the simple case where islands grow with a fixed shape. However, in several cases, bimodal island size distributions have been observed, inconsistent with classic coarsening [35]. A rich body of subsequent work showed that, in equilibrium, small islands are square pyramids or exhibit a dome-like shape, while larger islands develop a more complex multifaceted shape after passing through a first-order shape transition [40]. Several technological growth methods have been applied for the fabrication of such types of islands and nanostructures, in particular, molecular beam epitaxy [26], chemical vapor deposition [35], liquid-phase epitaxy [28, 14, 2, 12, 15] and other technological methods and approaches. As it was mentioned above, the mid-infrared spectral range of 3-5 μm has many important applications. The importance of this range attributes to the atmosphere transmission or the absorption spectra of some industrial gases. To satisfy the demands of state-of-the-art infrared photodetectors, quantum well infrared photodetectors (QWIP) and QDs infrared photodetectors (QDIP) are of great interest. QDIPs are predicted to have superior performances compared to QWIPs [37, 31], such as sensitivity to normal incidence infrared radiation, low dark current, high responsivity and detectivity. Many semiconductor material systems such as (In,Ga)As/GaAs, In(As,Sb)/GaAs and InAs/GaAs were investigated for QDIPs [5, 22, 24]. On the other hand, (Hg,Cd)Te (MCT) is a well-established solid solution, which has been the dominant system for mid- and far-infrared photodetectors. However, MCT suffers from instability and non-uniformity problems over larger area due to the high Hg vapor pressure. Theoretical studies predicted that only type-II superlattice photodiodes and QDIPs, as in our case, are expected to compete with (Hg,Cd)Te photodiodes [29]. Ternary and quaternary solid solutions in the InAs-InSb-InP system could be discussed as alternative materials for mid-IR and in some cases for far-IR range. In this review paper, we present results of the growth, characterization and electronic

properties of In(As,Sb,P) composition strain-induced micro- and nanostructures. Growth features and the shape transformation of pyramidal islands, lens-shape and ellipsoidal type-II quantum dots (QDs), quantum rings and QD-molecules will be under consideration. It will be shown that the application of quaternary In(As,Sb,P) composition wetting layer allows not only more flexible monitoring of lattice-mismatch between the wetting layer and an InAs(100) substrate, but also opens up new possibilities at nanoscale engineering and nanoarchitecture of several types of nanostructures.

2 Materials, Experimental Details, and Technological Approach

It is generally accepted that liquid phase epitaxy (LPE), which is an equilibrium growth technique, produces epitaxial material of the highest crystalline perfection containing few point defects and impurities only and is therefore well-suited for optoelectronic and other semiconductor devices fabrication. However, it is generally thought to be unsuitable for the growth of quantum-wells, QDs and other nanostructure. The main arguments against conventional LPE relate to the high initial growth rate which results in poor thickness control and reproducibility for thin layer epitaxy. However, as the results of many technologists show, it is possible to use LPE to grow multilayer III-V structures which exhibit quantum size effects [20], and with appropriate modifications and application of some technological know-how, LPE has been successfully employed to grow quantum-well heterostructure lasers [9, 32], nanostructures and nanostructure-based devices.

The main driving force at the nanoengineering and nanoarchitecture of In(As,Sb,P) composition strain-induces nanostructures is the surface diffusion of antimony atoms, like in classic InAs/InSb system. But the presence of the phosphorous atoms and their surface diffusion to one or the opposite direction in our quaternary material system opens up a new possibility and can be employed as an additional tool to control the nucleation process and the type of nanostructure. Physically and technologically we propose and assume the following scenario: depending on the growth conditions (growth temperature, composition of the liquid phase and its contact time with the substrate surface, etc.), when for example for the phosphorous atoms it is energetically preferable to jump out from the QD, nanopits will nucleate around the QD [14]. Otherwise, when phosphorous atoms are energetically preferable to move to the center of QD, the final shape of the nanostructure will be a quantum ring (QD with the pit on the top). In this case, quantum rings are not surrounded by the pits. Thus, at the initial composition of the quaternary liquid phase when the epi-layer and the InAs(100) substrate are lattice matched, monitoring of the antimony and phosphorus concentration allows not only more flexible control of the difference between the wetting layer and the substrate lattice constants, but also it sign. In particular, with increasing the antimony concentration (with respect to the lattice-match composition) the wetting layer acquires a convex form, while with increasing the phosphorus concentration it becomes concave. Therefore, depending on the relaxation mechanism of the elastic stress, different types of nanostructure can be nucleated. In all our experiments, the samples were grown using LPE slide-boat crucible. The thickness of the liquid phase was 500 μm. The whole growth process was performed within a purified hydrogen atmosphere. The industrial InAs crystals used as substrates were 11 mm in diameter and 400 μm thick, (100) oriented, undoped, having background electron concentrations of 2×10^{16} cm^{-3}. For the growth solution formation the 7N indium, 6N antimony, undoped InAs and InP crystals were used. High-resolution SEM (SEMEDXA-FEI Nova 600-Dual Beam), AFM (TM Microscopes-Autoprobe CP), TEM and STM techniques were used for nanostructure characterization. Fourier-transform infrared spectrometry (FTIR-Nicolet/NEXUS) and an IRS-21 spectrometer were used to investigate the transmission and photoresponse spectra of grown structures, respectively. Electrophysical characteristics were measured using „Keithley-6514 System Electrometer“ and

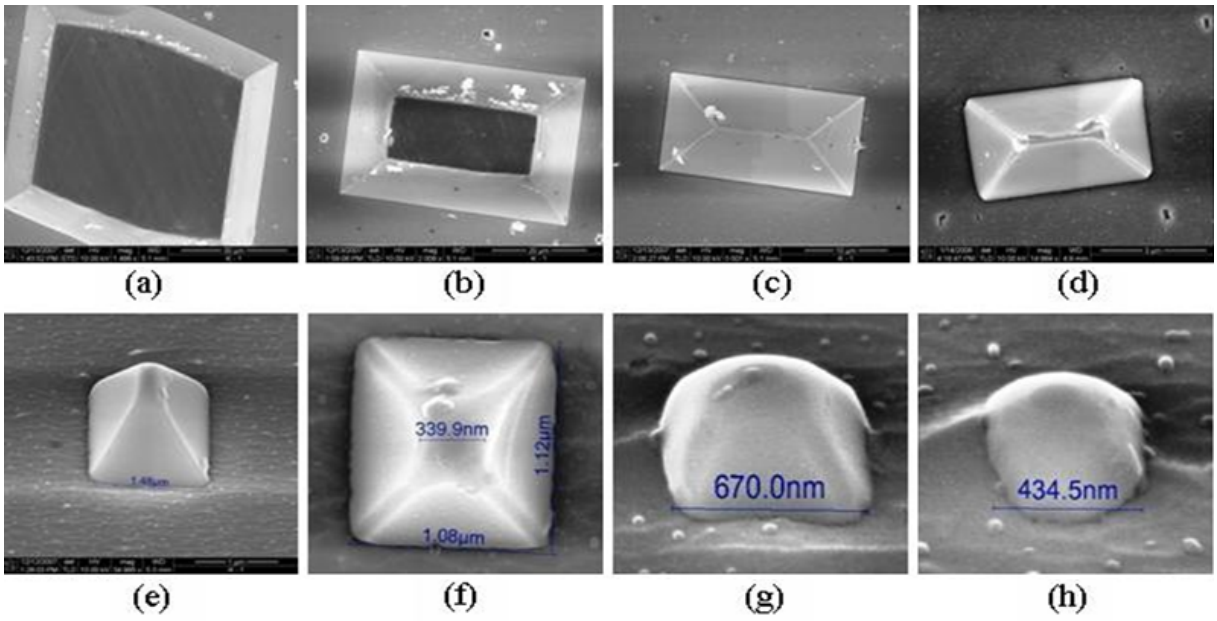

Figure 1: The self-assembled In(As,Sb,P) composition strain-induced islands grown from liquid phase on an InAs(100) substrate and their evolution from a truncated pyramid to a semi-globe.

„QuadTech-1920 precision LCR meter“.

3 Results and Discussions

3.1 he Growth and Characterization of In(As,Sb,P) Composition Micro- and Sub-Micrometric Strain-Induced Islands

As it was already mentioned, in contrast to other growth techniques as molecular beam epitaxy or metal organic chemical vapor deposition, LPE operates comparatively close to thermodynamically equilibrium. Within LPE, traditionally, the liquid phase is homogenized during 4 - 6 hours (in some cases even more) to equilibrate thermodynamically. In our first experiments, though, we performed some non-traditional approach with the purpose to grow nanostructures. We specially used an inhomogenized liquid phase (keeping the liquid phase at growth temperature of T=550oC just about one hour), but having a quaternary In-As-Sb-P composition which corresponds to an $InAs_{0.742}Sb_{0.08}P_{0.178}$ composition epilayer lattice matched with the InAs(100) substrate. The thickness of the liquid phase was equal to 8 mm. After that, the liquid phase was brought into contact with the substrate during ten minutes and removed from the substrate surface. The high-resolution SEM characterization revealed, from our point of view, very interesting micrometric and sub-micrometric strain-induced islands nucleated at the substrate surface, as presented in Figure 1.

Obviously, due to their dimensions, these islands are far away from being called QDs. However, from the crystallographic point of view, an interesting shape transformation with volume decrease is clearly visible: from truncated pyramids to semi-globes, which, as our further experiments show, then gradually evolve to lens-shape (or other configuration) QDs. The chronology of the shape transformation is schematically presented in Figure 2. According to the thermodynamic principle (minimum energy), during the growth on (100) or (001) faceted substrates, as the strain-induced islands volume decreases,

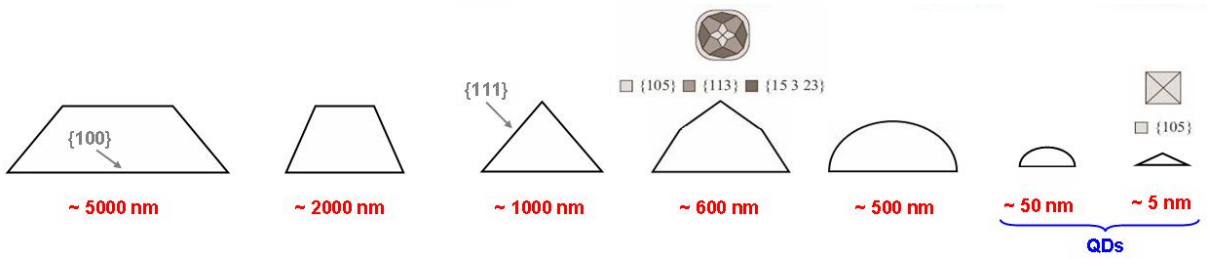

Figure 2: Shape architecture of strain-induced islands at volume decreasing.

the following succession of shape transitions has to be detected: truncated pyramid, {111} facetted pyramid, {111} and partially {105} facetted pyramid, completely unfacetted „pre-pyramid“, semi-globe like object, and then lens-shape or other geometry QD.

Consequently, LPE grown islands on (100) oriented surfaces exhibit a similar shape for an extended concentration range mainly consisting of truncated pyramids with 111 side facets and a 100 top facet with a nearly constant aspect ratio between the island base along (110) and the island height. Next, micrometric and sub-micrometric pyramids were cut-off using a focused ion beam (FIB) in high vacuum. For the analysis of the QDs composition, energy dispersive X-rays analysis (EDXA) was applied [15]. After rotating the whole sample, cross-sectional SEM-EDXA measurements from the two opposite angles at the top and bottom of the pyramids were performed. Taking into account the penetration depth and using the electron probe point microanalysis, the following X-ray lines are detected: In-L(α), As-L(α), Sb-L(α), P-K, which we use to perform a quantitative spectral analysis at an electron energy of 10 keV. Acquisition time is 5 s per spectrum. The results of measurements show that the compositions and lattice mismatch ratio exhibit good symmetry values in both angles of the base of the cut-off pyramids. Additionally, the results show that the strength (lattice mismatch ratio with the InAs substrate) at the top of the pyramids is smaller than at its bottom angles, and that the islands size becomes smaller when the lattice mismatch increases. Finally, as already was mentioned, the liquid phase was homogenized just for one hour at the LPE initial growth temperature. A longer time (approx. 6 h and more) or a multistage homogenization of the liquid phase should prevent micrometric and sub-micrometric islands formation and/or allow their suppression, thereby favoring QDs formation.

3.2 The Growth and Characterization of In(As,Sb,P) Composition Type-II Lens-Shape and Ellipsoidal QDs

In this section we will describe the growth process of quaternary liquid phase In(As,Sb,P) composition lens-shape and ellipsoidal QDs and their characterization. Three samples were prepared for investigations. The first and second samples consist of unencapsulated lens-shaped and ellipsoidal QDs grown on InAs(100) substrate, respectively. The third sample is a n-InAs/p-In(As,Sb,P) diode heterostructure with QDs embedded into the p-n junction spatial charge region. Both QDs and the epitaxial p-In(As,Sb,P) epilayer with 4 μm of thickness were grown by LPE with a modified slide-boat crucible at initial growth temperature of T=550°C. The thickness of the liquid phase was chosen to be equal to 500 μm, in order to prevent the influence of convection and temperature gradients on the growth process. Our investigations show that this technological approach increases the reproducibility of the grown structures. According to the InAs-InSb-InP quasiternary phase diagram, as a starting point, we use the quaternary liquid phase composition that corresponds to the $InAs_{0.81}Sb_{0.06}P_{0.13}$ alloy in solid phase, that is conveniently lattice-matched to InAs substrate. QDs were grown at isothermal conditions, but the concentrations of antimony and phosphorus in the growth solution were chosen to

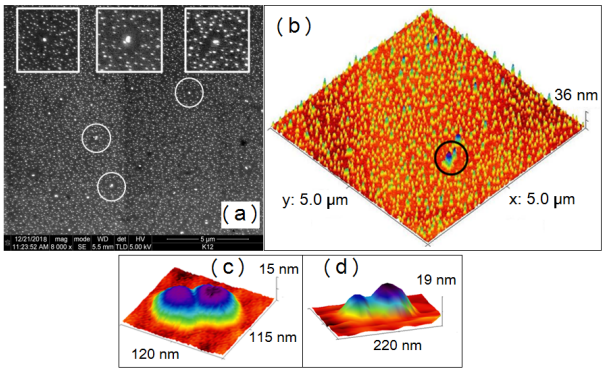

Figure 3: (a), (b) - HR-SEM (S = 17×17 μm^2) and AFM images of InAsSbP QDs grown by LPE on InAs (100) surface (sample 1), respectively; (c), (d) - AFM topography images of QDs coalescence and coarsening.

provide a lattice mismatch of up to 3% between the InAs substrate and the In(As,Sb,P) wetting layer at T=550°C. QDs for the sample 1 and sample 2 were nucleated under the same technological conditions, but at different contact duration of the liquid phase with the substrate: t_1= 10 min and t_2= 30 min, respectively. The third sample was prepared by two steps in a single technological process using two liquid phases. First, QDs were nucleated on the epi-ready substrate surface at isothermal conditions (t_1=10 min). Then the liquid phase was changed and the p-In(As,Sb,P) epilayer was grown by step-cooling version of LPE at ΔT=8 K to provide 4 μm of epilayer thickness.

The SEM and AFM images of the surface of sample 1 are presented in Figure 3 (a) and Figure 3 (b), respectively. The enlarged view of regions denoted in Figures 3 (a, b) by white and black cycles are presented as insets in Figure 3 (a). The bimodal growth mode is visualized in Figure 3(a, b). The size distribution of the QDs shows uniform distributed small QDs in sufficiently large (approx. 300 μm^2) areas while large QDs are rarely distributed. Statistical evaluations show that the area density of small and mainly lens-shape dQDs ranges from 6 to 8×10^9 cm^{-2}, with heights from 0.5 nm to 25 nm and widths from 10 nm to 40 nm. Otherwise, the average density of large QDs is up to three orders of magnitude lower, with the average height and diameter of approx. 30 nm and 70 nm, respectively. From HR-SEM and AFM images we conclude: (i) the large QDs are free from small QDs in their surrounding area (the Ostwald ripening process) (Figure 3 (a) insets), and (ii) coalescence and coarsening of QDs (Figure 3 (c, d)) occurs. In the S-K growth mode the last stage of nucleation in solid and liquid solutions is often characterized by the growth of largest (supercritical) clusters and dissolving of small (subcritical) ones. This results in the decrease of the density of clusters with the increase of their respective sizes. Such a process of coarsening of clusters is usually termed in literature as Ostwald ripening in connection with his studies performed as early as in the beginning of 20-th century [30]. The first adequate theoretical justification of this phenomenon was done by Lifshits and Slezov in 1958 [25] and was then extended by Wagner [43]. Analysis shows that small QDs are mainly lens-shape, but the larger ones (starting from approx. 60 nm) are ellipsoidal with the elongation mainly along [010] direction. HR-SEM and AFM images of the ellipsoidal In(As,Sb,P) QDs (sample 2 surface) are presented in Figure 4 (a) and Figure 4 (b, c), respectively, with the corresponding AFM line scans passing through the ellipsoidal QDs denoted in Figure 4 (b, c).

The ellipsoidal QDs average density is equal to (5-8)×10^8 cm^{-2}. By the statistical analysis of the AFM measurements we estimate elongation ratios (L_X / L_Y = 1.23 $\pm$ 0.12, L_X / L_Z = 9.2 $\pm$ 3.6 and L_Y / L_Z = 7.9 $\pm$ 3.5) in all three directions, where L_X, L_Y and L_Z are the lateral semi-axis and the height of QDs, respectively. Thus, investigations show that the ellipsoidal QDs are weakly prolate in

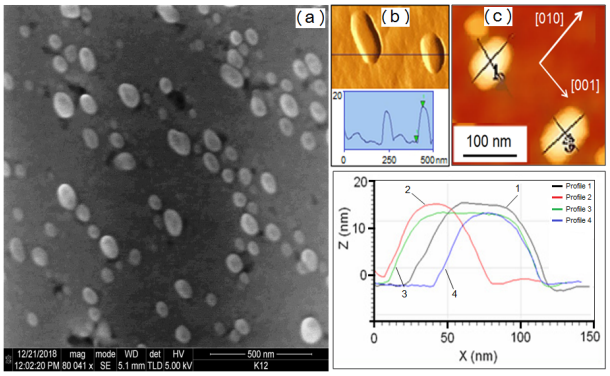

Figure 4: High resolution SEM image (a) of the ellipsoidal In(As,Sb,P) QDs grown by LPE on an InAs (100) surface (sample 2) (S = 1.7×1.7 μm^2), (b), (c) - AFM images with line scans.

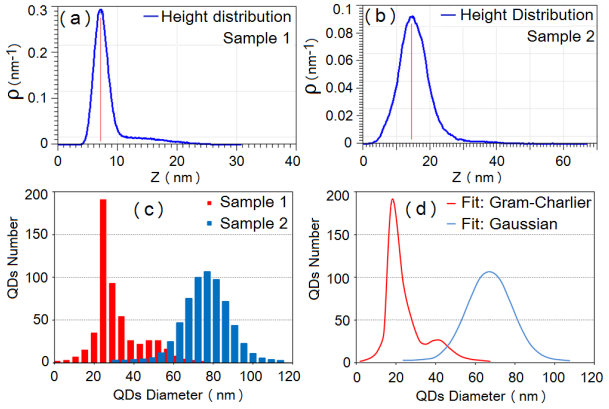

Figure 5: (a), (b) - QDs' heights distribution for the sample 1 and sample 2 (S = 5×5 μm^2); (c), (d) - the QDs histograms and approximation fits by the Gram-Charlier function (sample 1) and the Gaussian (sample 2), respectively.

[010] direction and strongly oblate in [001] direction. Consequently, a strong localization of the charge carriers (light holes in our type-II In(As,Sb,P) QDs material system) perpendicular to the substrate surface is physically expected. We also detected the linear dependence of L_X / L_Y versus L_X. The linear approximation of experimental data is performed and the cross point of $L_X \approx 55$ nm with the line L_X / L_Y = 1 is calculated. We suggest that the elongation of spherical QDs is started mainly from this size. The QDs' heights distribution for the sample 1 and sample 2, histograms of the QDs' number versus their average diameters with approximation curves are presented in Figure 5.

It can be seen from Figure 5 that: (i) bimodal distribution for the QDs' number versus either height or diameter reveals for the sample 1 (Figure 5 (a) and 5 (c)), and (ii) transformation of the QDs' histograms and distribution functions occurs with increasing growth time. In particular, the QDs' distribution for sample 1 is well fitted by the Gram-Charlier function, but for sample 2 by a Gaussian (Figure 5 (d)). Using the time dependence of the QDs' average diameter (optimal values), we evaluated the average radial nucleation rate for our QDs, which is equal to 0.05 nm/s. Figures 6(a) and 6(b) show the photoluminescence (PL) spectra of all three samples at T=78 K and the room temperature electroluminescence (EL) spectra of sample 3 at different direct currents passing through the p-n junction, respectively.

The EL spectra were measured from a diode mesa-chip with an area of 0.2 mm^2, which was formed by etching in methanol solution with 25 vol. % of Br. This is the typical size of only one standard

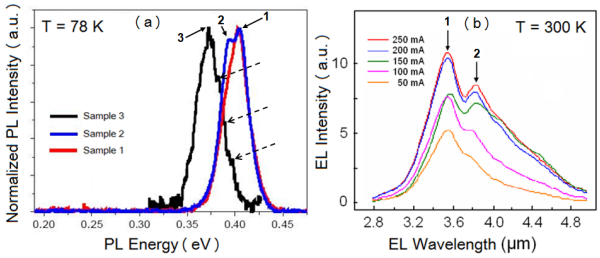

Figure 6: (a) - the PL spectra of all three samples at T = 78 K, and (b) - the room temperature EL spectra of sample 3 at different direct currents passing through the p-n junction.

segment usually used for designing infrared photodetectors. The band gap energy for p-In(As,Sb,P) epilayer was specially chosen be equal to 0.48 eV at T=78 K in order to provide either „optical window“ or localization also of the electrons (due to the potential barrier) along with the holes inside the capsulated type-II QDs. Actually, in sample 3 type-II In(As,Sb,P) QDs must exhibit the physical properties appropriated to type-I QDs. For samples 1 and 2, only one PL peak reveals (peak 1 in Figure 6 (a)) coincidence to the band-gap energy for the undoped InAs (E=0.404 eV) at liquid nitrogen temperature. This means that the radiative recombination of the electron-hole pairs occurs in the InAs substrate outside the uncapped QDs, due to the spatial separation of excited electrons and holes in type-II QDs. Nevertheless, we do not expect recombination inside the QDs, but in that case the PL signal suppression probably happens due to electron-phonon interaction and scattering. Theoretical calculations show that in In(As,Sb,P)-based QD structures, however, due to a shallow barrier a weak localization of electrons is also possible [28]. In sample 3, a p-type cap layer creates a potential barrier for the exited electrons and the probability of direct radiative recombination inside the QDs sufficiently increases, which is confirmed by peak 2 (E=0.371 eV) appearing and a shift og peak 1 of up to 33.2 meV. Next, the second sample's magnetic field dependence of the electric sheet resistance (magnetoresistance) was measured in Faraday geometry at room temperature as well as at liquid nitrogen temperature. Measurements were performed at gradually increasing magnetic field of up to 1.6 T, subsequently decreasing to zero. Magnetoresistance curves for our In(As,Sb,P) type-II QDs at room and T=78 K temperatures are presented in Figures 7 (a, b), respectively. Figure 7 (c) shows the derivative of room temperature magnetoresistance curve measured at increasing magnetic field.

From Figures 7 (a-c) the periodic fractures on magnetoresistance curves, oscillations of the derivative curve with the period of ΔB $\approx$ 0.36 $\pm$ 0.03 T, as well as the sheet resistance hysteresis of ΔR $\sim$ 50 mΩ (ΔB = 0.255 T) and Δ R $\sim$ 400 mΩ (ΔB = 0.421 T) at room and T=78 K temperatures, respectively, are glaring. Actually, type-II QDs and QRs are distinctly different from single or multiple stacked Type-I QDs in that they have a not simply-connected geometry and that the charge carrier distribution is more complicated. For both cases, this geometry defines a ring-like trajectory for electrons (or holes) in the magnetic field depending on band alignments. In our type-II QDs, for instance, holes are strongly localized inside the QDs, but the electron's wave function is „pushed“ outside of the dot, as we have confirmed in previous calculations based on an eight-band $\mathbf{k}\cdot\mathbf{p}$-simulation [28]. A schematic band structure in [001] direction and the model for an electron-hole pair in a type-II In(As,Sb,P) elongated QD in magnetic field is presented in Figure 7 (d). Evidently, the magnetic flux leads to a periodic change in the quantum mechanical properties of the encircling electrons. Therefore, upon the application of a magnetic field, the electron orbits the QD periphery producing an observable Aharonov-Bohm effect (ABE) [1]. Rotation of the electron results in a periodic switching of the ground state with the angular momentum l_e = 0 to $l_e \neq 0$, in specific windows of the magnetic field, as it is presented in Figure 7 (c). However, in Figure 7 (c) four well-resolved oscillations with the period of ΔB $\approx$ 0.377 T are evi-

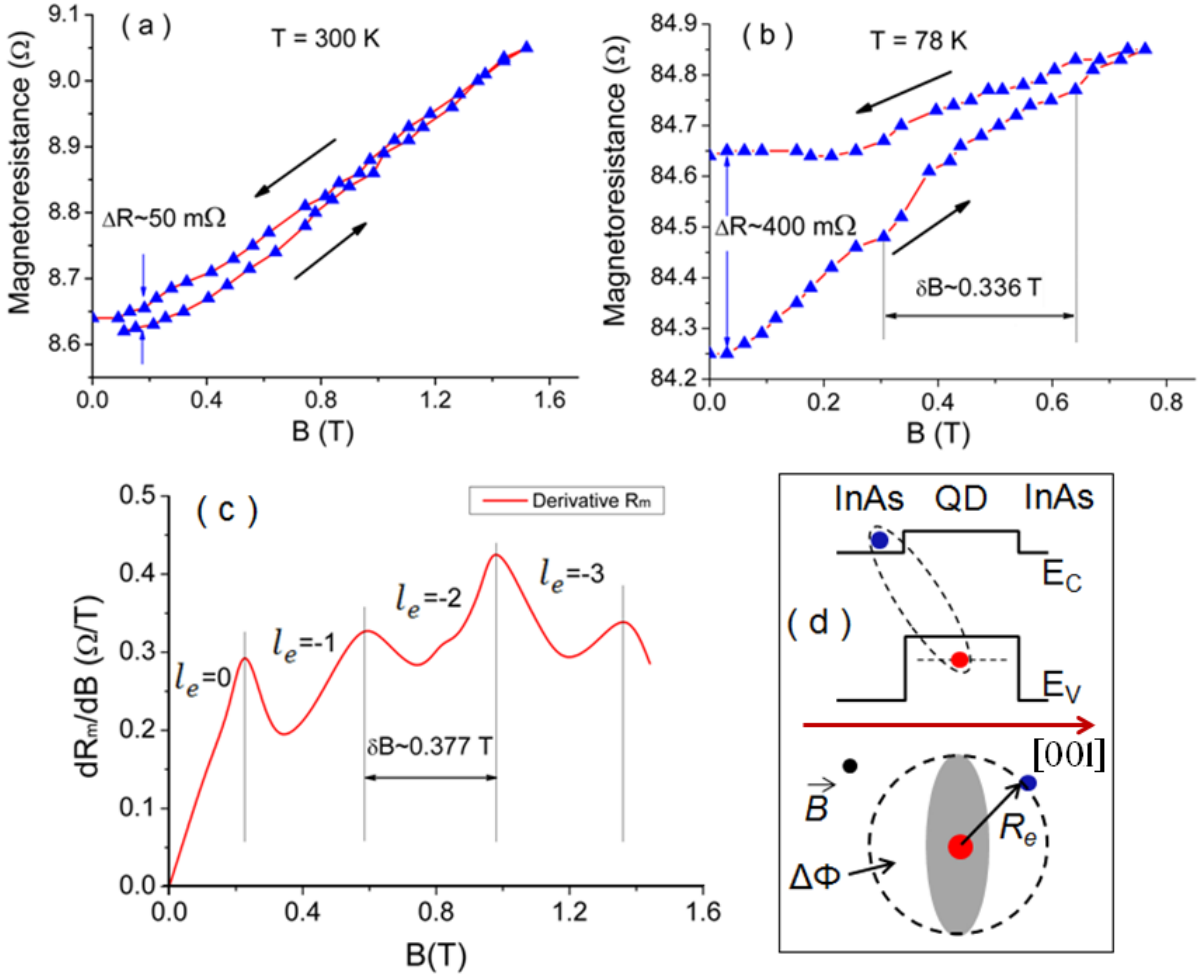

Figure 7: (a, b) - the second sample's sheet resistance versus magnetic field at Faraday (perpendicular to the substrate surface) geometry at room and liquid nitrogen temperatures, respectively; (c) - derivative of (a); (d) - schematic band structure in [001] direction and the model for an electron-hole pair in a type-II In(As,Sb,P) elongated QD.

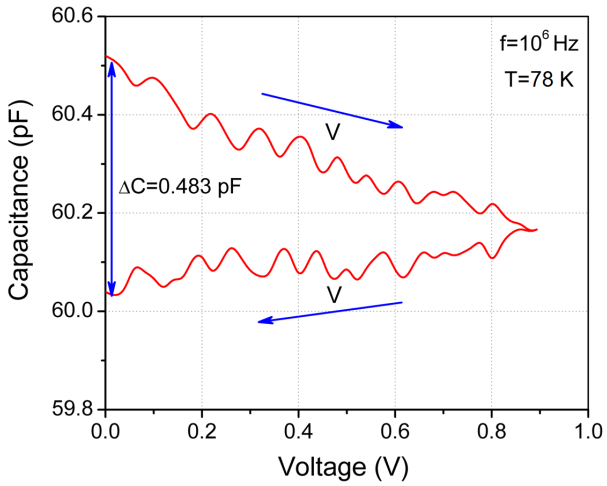

Figure 8: The capacitance - voltage characteristic at T = 78 K and f = 10^6 Hz frequency.

dent. Since the period of oscillations should be approximately given by Δ B = $4\Phi_0/\pi D_e^2$ [10, 21, 33], where Φ_0 = h/e is the quantum flux, a diameter of D_e = 120 $\pm$ 10 nm is obtained. This value for the electron's circling diameter is reasonable and coincides with the ellipsoidal QDs diameter in [010] direction (AFM line-scans in Figure 4). The selection rules for transitions in angular momentum are strictly valid only for the situation of perfect rotational symmetry and low temperatures (less than the temperature of thermal ionization of the exciton). Nevertheless, we assume that ABE oscillations are probable in our QDs system [19] and that electrons perform the circular motion around the elongated QDs, since the substrate (matrix) is a high quality and undoped InAs crystal, where the probability of electrons scattering on impurity or dislocation is negligibly small. Next, in order to definitely state that only the influence and contribution of QDs are responsible for the observed oscillations, we also measured the capacitance-voltage (C-V) characteristics using High Precision Capacitance Spectrometry (QuadTech-1920 precision LCR meter). To do so, we prepared a device structure in the form of a photoconductive cell (PCC) with an active surface area of 1 mm^2. The topology of the ohmic contacts was chosen to provide needed requirements for the PCCs. The results of the C-V measurement performed at T = 78 K and f = 10^6 Hz frequency are presented in Figure 8 [16].

The C-V characteristic was measured continuously at increasing applied voltage from 0 to 0.9 V with subsequent decrease to 0, as denoted in Figure 8. Figure 8 shows that, (i) oscillations in the C-V curve are observed, (ii) these oscillations are opposite-directed at increasing and further decreasing of the applied voltage, and (iii) capacitance hysteresis of Δ C = 0.483 pF is observed. We suppose that the revealed C-V opposite-directed oscillations occur due to the structure's total charge oscillations, which is caused by the depletion and occupation of the QDs energy levels. The detected hysteresis can be explained by the remnant polarization in the structure due to spatial separation of the charge carriers in type-II QDs, which is conserved after shut off the applied voltage. Light holes from the first state can be emitted by direct tunneling through the triangular barrier, and/or from the first state are thermally activated into excited states and subsequently emitted by thermal and tunnel emission, whereas heavy holes are emitted by pure thermal activation from the first state into the InAs substrate's valence band.

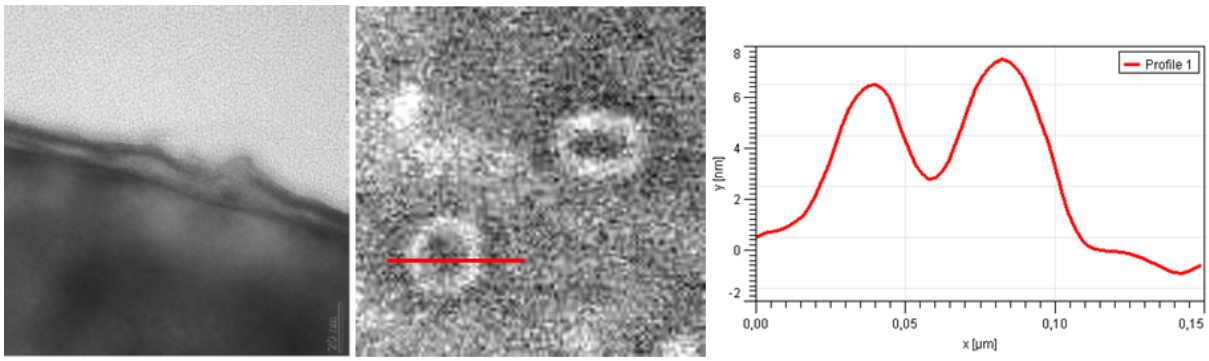

Figure 9: (a) - TEM, (b) - HR-SEM and (c) - AFM line-scan images along of QRs grown by LPE on an InAs (100) substrate along the red line marked in (b).

3.3 The Growth and Characterization of In(As,Sb,P) Composition Quantum Rings and In(As,Sb)/In(As,P) QD-Molecules

Ring-shaped semiconductor nanostructures and so-called QDs-molecules have gathered growing attention in recent years [14, 10]. These structures have many interesting electronic properties and confine carriers into ring-like quantum states [10]. Quantum rings (QRs) also provide a means to study quantum effects involving magnetic flux. Most of the experimental works in this field were performed using mainly MBE and MOCVD techniques. However, as our experiments show, the LPE technique at quaternary composition liquid phase can also be successfully used for nanoengineering of QRs [17] and QDs-molecules [14] in the form of a „nano-camomile“. QRs were grown from the quaternary In-As-Sb-P liquid phase of 500 μm in thickness and contact duration with the substrate of 20 min. Concentrations of phosphorus and antimony in liquid phase were chosen twice as high as those at the growth of QDs. AFM statistical exploration shows that the QRs' average density is equal to (1-3)$\times 10^9$ cm^{-2} with the average height and outlet diameter of 10 nm and 35 nm, respectively. Gauss-like distribution on the dependence of QRs number versus average outlet diameter was observed. QRs TEM, HR-SEM and AFM line-scan images are presented in Figure 9.

Type-II QDs and QRs are distinctly different from single or multiple stacked type-I QDs and the charge carrier distribution and their geometry is more complicated. This geometry makes them particularly interesting for studies in magnetic fields, because for both cases this geometry defines a ring-like trajectory for electrons (or holes), ensuring that for instance in our type-II In(As,Sb,P) QDs and QRs the electron wave function is delocalized, as we have confirmed in previous calculations based on eight-band $\mathbf{k} \cdot \mathbf{p}$-simulations [28]. Here, the free particle is the electron rather than the hole, which has a smaller effective mass. A strong band gap bowing in In(As,Sb) induces a shallow conduction band minimum in In(As,Sb). However, strain effects in the systems studied in Ref. [3] due to the lattice mismatch to the surrounding InAs matrix compensate for this minimum in the conduction band offset and prevent an electron localization in the In(As,Sb) QDs and QRs. The magnetic flux leads to a periodic change in the quantum mechanical properties of the charge carrier system in QR and encircling the type-II QD. These oscillations are periodic in the applied magnetic field and are known as Aharonov-Bohm oscillations as mentioned above.

We investigated the magnetic field dependence of the electric sheet resistance (magnetoresistance) for QRs samples at the Faraday (perpendicular to the substrate surface - Z) and Voigt (parallel to the substrate surface - X and Y) geometries. A magnetic field of up to 1.6 T was applied and measure-

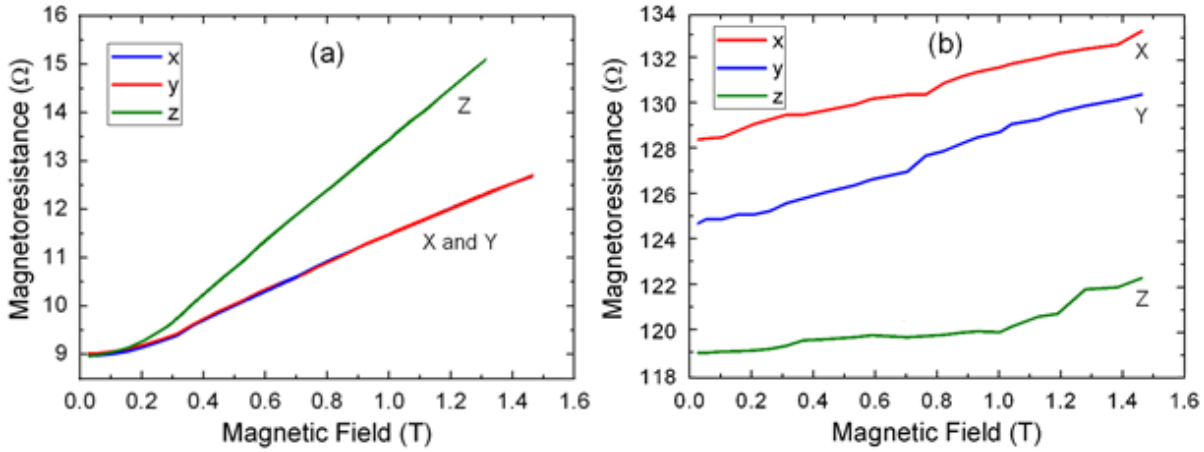

Figure 10: Sheet resistance (magnetoresistance) versus magnetic field at Faraday (perpendicular to the substrate surface - Z) and Voigt (parallel to the substrate surface - X and Y) geometries of InAs substrate (test sample) - (a) and structure with QRs - (b).

ments were performed at room temperature. The classical behavior of the dependence of the electric sheet resistance versus the magnetic field was measured and observed for the InAs substrate as a test sample (Figure 10 (a)). Otherwise, for the QRs-based sample, specific fractures (probably due to the AB effect) on the magnetoresistivity curve are revealed and detected (Figure 10 (b)). Figure 10 also reveals that the values of the QRs sample's sheet resistance are higher up to one order of magnitude as compared to the reference sample.

Next, while quaternary composition In(As,Sb,P) QDs with several shape geometry have been successfully grown as it was mentioned above, however, only a few studies on quaternary cooperative QDs/leaves structures, so-called „nano-camomiles", as a new type of QDs molecules have been reported so far [14, 2]. In our experiments, at the growth of In(As,Sb)/In(As,P) QD molecules the main driving force at nucleation was the surface diffusion of antimony atoms, similar to that in classic InAs/InSb-systems. This leads to the formation of In(As,Sb)-QDs. Simultaneously, phosphorous atoms move to the surrounding material around the In(As,Sb)-QD, thus forming the surrounding In(As,P) QDs that we refer to as leaves, and therefore forming a coupled In(As,Sb)/In(As,P) dot-leaf nanostructure. Detailed technological conditions at the growth of „nano-camomiles" are described in Ref. [14] and [2]. STEM, HR-SEM and AFM characterizations show that our QDs molecule consists of central In(As,Sb)-QD surrounded by mainly six In(As,P) leaves as it is seen from Figure 11.

While charge carrier localization is expected in the central In(As,Sb)-QD rather than in the surrounding In(As,P) leaves in these „nano-camomiles", due to the conduction and valence band offsets of the dot, leaves and surrounding matrix material, long-ranged strain, and polarization potentials arising from the leaves are expected to induce a significant influence on the properties of the electrons and holes in the central dot. Controlling the composition ratio between As, Sb, and P in liquid phase allows strain control in In(As,Sb,P), and therefore a modification of the growth process and structural properties of the In(As,Sb) dots and the surrounding In(As,P)-leaves.

The room temperature FTIR spectrum of uncapped In(As,Sb,P) QD/leafs structure grown on InAs(100) by LPE is presented in Figure 12. As a test sample, we use the same undoped InAs(100) substrate without In(As,Sb) QDs and surrounding In(As,P) leaves. The results show the displacement of the absorption edge toward the long wavelength region from 3.44 μm (for the test sample) to 3.85 μm. We assume that this effect is the result of the absorption by the QDs through the permitted energy sub-band. Even though the shift of the absorption edge clearly indicates the optical activity of the

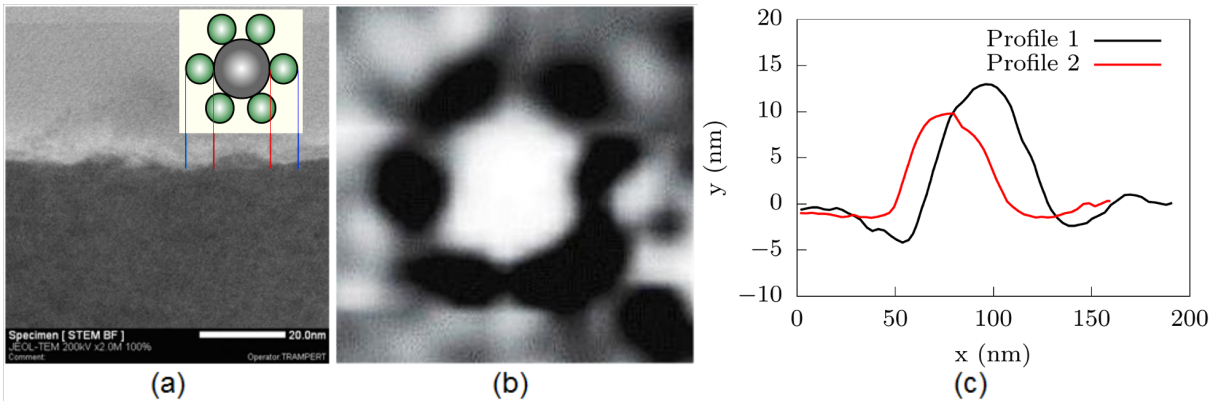

Figure 11: STEM - (a), HR-SEM - (b) top view image of a cooperative QDs/leaves structure (c) AFM line scan along two different axes. The inset in (a) shows a schematic view of the structure with the In(As,Sb) dot being indicated in gray and the In(As,P) in green.

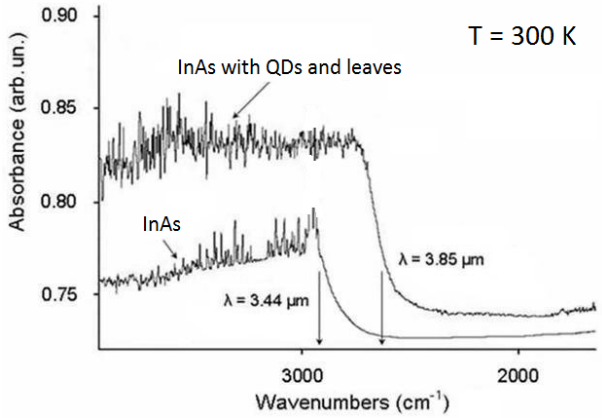

Figure 12: Room temperature FTIR spectra of the InAs test sample and the In(As,Sb,P) QD/leave structure sample.

nanostructures, discrete emission peaks are not clearly distinguishable in the spectrum. We account this to the fact that the spectrum was measured at room temperature and to the presence of the larger, probably ellipsoidal QDs. Future investigations of the In(As,Sb)/In(As,P)-nanostructures will therefore require low-temperature photoluminescence measurements.

Obviously, our QDs molecules are an excellent subject for understanding the complicated influences of strain, polarization potential, and band offsets on the electronic structure of coupled In(As,Sb)/In(As,P) nanostructures. To achieve a more detailed understanding of the electronic properties of these nanostructures, a theoretical description based on the experimental observations is required, allowing to study the influence of experimentally tunable parameters of the In(As,Sb)/In(As,P) nanostructures on their electronic properties and to identify possible applications of these systems. This will be the subject of the next section.

3.4 Simulations of the Electronic Properties of Nanostructures Using an Eight-Band $\mathbf{k} \cdot \mathbf{p}$ Model

We have systematically investigated the electronic properties of LPE-grown In(As,Sb,P) nanostructures using an eight-band $\mathbf{k} \cdot \mathbf{p}$-model for zincblende crystals [4]. Our modelling takes elastic and

piezoelectric properties of semiconductor heterostructures into account and is implemented within the plane-wave framework of the Sphinx physics library [7, 27, 11]. The respective material parameters for the ternary and quaternary alloys were consistently taken from Ref. [42]. In a first work, we have studied the single-particle electronic properties of an In(As,Sb)-In(As,P) cooperative QD/leaves nanostructure [28]. We have shown that, while holes are confined in the In(As,Sb) central QD, electrons do not localize in the specific heterostructure that was subject of this study, but their localization features can be easily tuned by strain or additional electrostatic potentials [28]. Respective hole charge densities in such an In(As,Sb)-In(As,P) cooperative QD/leaves nanostructure are shown in Figure 13 a. A more recent study has aimed for a systematic investigation of the electronic properties of In(As,Sb,P) graded-composition quantum dots (GCQDs) in close comparison to the experiment[18].

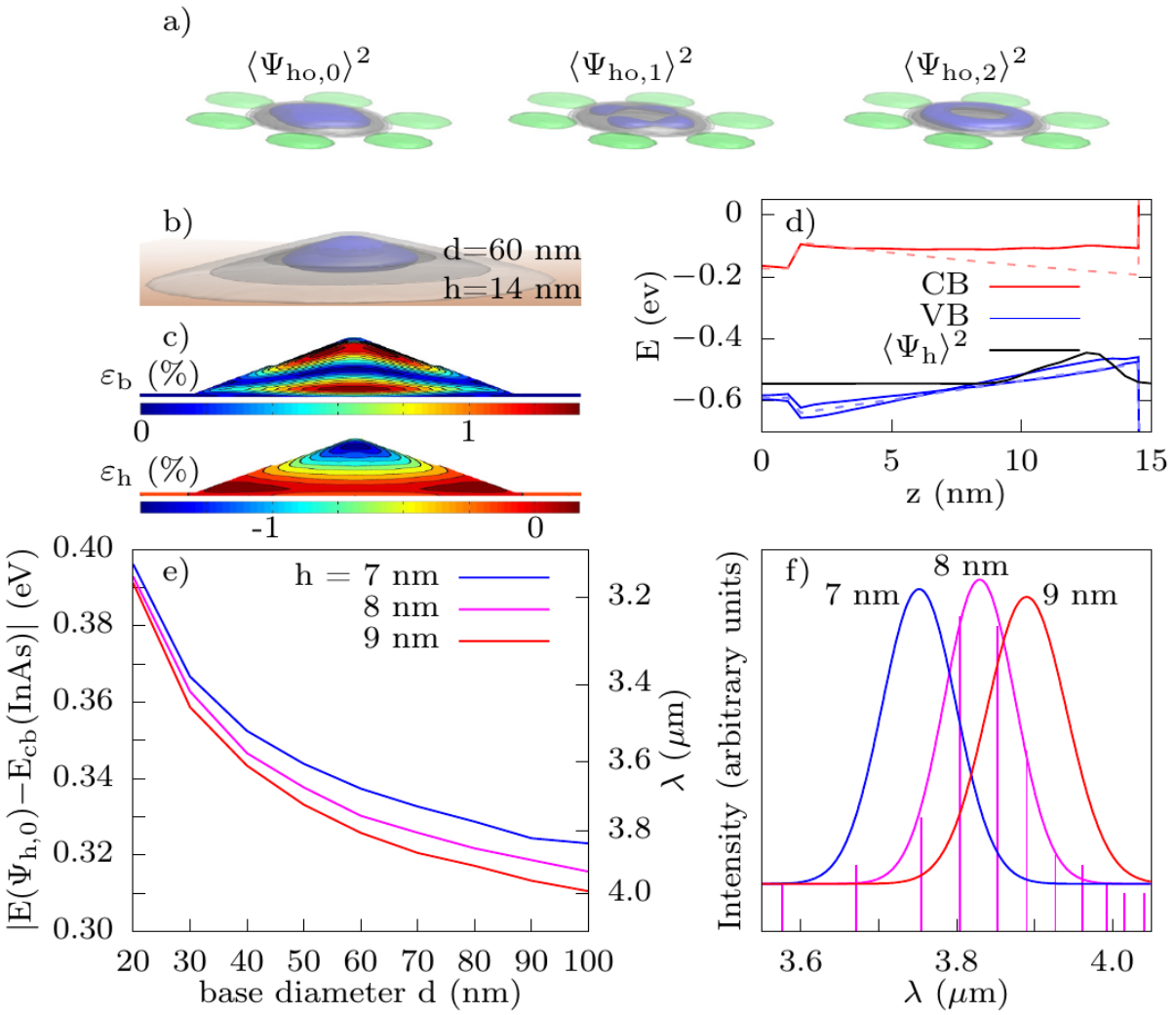

Figure 13: a - hole charge densities inside an In(As,Sb,P) nano camomille. Green isosurfaces depict the In(As,P) leaves, gray shaded isosurfaces the central In(As,Sb) QD. The hole charge density is marked in blue. b - hole ground state charge density of an example In(As,Sb,P) GCQD. Biaxial and hydrostatic strain maps are shown in a side view in c. d: Band profile along the central axis of an In(As,Sb,P) GCQD. Conduction and valence bands are depicted in red, and blue, respectively, a black solid line indicates the hole ground state charge density. The band profile under neglection of strain is indicated in dashed lines. e - Transition energy between hole ground state and electron continuum as a function of the GCQD diameter for different heights. f - simulated ensemble spectra for GCQDs of different heights.

A typical GCQD is shown in Figure 13 b in a perspective view. White-to-gray shadings mark the increasing Sb content from the GCQDs bottom to top, and the hole ground state charge density is shown in blue. The respective biaxial and hydrostatic strain components of this system are shown below (Figure 13 c). While the InSb content of the In(As,Sb,P) content might facilitate electron confinement at the GCQDs top, the strain distribution throughout the system modifies the conduction band to an almost flat-band case with its minimum being clearly in the InAs substrate, as can be seen in Figure 13 d. We have then systematically studied hole state confinement and transition energies between hole ground state and the electron continuum for GCQD diameters and heights as observed in experiment. The respective single-particle energies derived from the eight-band $\mathbf{k} \cdot \mathbf{p}$-model were corrected to room temperature using Varshni's correction [41] and the resulting transition are shown as a function of the GCQD diameter for heights as observed in experiment in Figure 13 e. Finally, we have mapped these energies onto the histogram of GCQD diameters observed in order to obtain an ensemble absorption spectrum, shown in Figure 13 f. The agreement between the simulated spectrum for h = 8 nm is astonishingly good (3.829 μm vs. 3.83 μm measured via FTIR spectroscopy), whereas a deviation of 1 nm in GCQD height already induces a significant blue (3.752 μm for h = 7 nm) or red shift (3.890 μm for h = 9 nm). We note that our modelling scheme appears best suited to facilitate theory-driven design for In(As,Sb,P) heterostructures that exhibit compositional grading.

3.5 Fabrication and Investigation of Mid-Infrared QDs Photodetectors

In this section we present the following two mid-infrared photodetectors prepared for investigations. Structure 1 (Figure 14 (a)) is the photoconductive cell (PCC) based on commercial undoped n-InAs(100) substrate with an electron background concentration of 2×10^{16} cm^{-3} and an electron mobility of 45000 cm^{2}V^{-1}s^{-1} at T=78K and the unencapsulated lens-shaped QDs grown on the substrate surface. Structure 2 (Figure 14 (b)) is an n-InAs/p-In(As,Sb,P) diode heterostructure with QDs embedded into the p-n junction spatial charge region. Both QDs and epitaxial p-In(As,Sb,P) epilayer with 4 μm of thickness were grown from a quaternary In-As-Sb-P liquid phase by LPE with a modified slide-boat crucible at initial growth temperature of T=550°C. The second sample was prepared by two steps in a single technological process using two liquid phases. First, QDs were nucleated on the epi-ready substrate surface at isothermal conditions (t=10 min). Then the liquid phase was changed and the p-In(As,Sb,P) epilayer was grown by step-cooling version of LPE at ΔT=8 K to provide 4 μm of epilayer thickness. The ohmic contacts to both structures were fabricated by traditional vacuum evaporation technique in the form of Au(Ge)/Cr sandwich with further thermal annealing. Geometric configuration and topology of the ohmic contacts were chosen to provide a uniform current flow. In Figures 14 (c) and 14 (d) photos of the sample taken from LPE crucible and capsulated (TO-5) mid-IR photodetectors are presented, respectively.

HR-SEM and TEM images of In(As,Sb,P)-based QDs mid-infrared diode heterostructures cross sections are presented in Figure 15 (a) and (b), respectively. The samples' optoelectronic properties were first characterized using photoresponse measurements at room temperature with a variety of excitation wavelengths using a standard globar source and NaCl beam splitter. Room temperature normalized photoresponse spectra of the QDs PCC (Structure 1) in combination with the InAs test sample and a diode heterostructure (Structure 2) are presented in Figure 15, respectively. For the crystalline undoped InAs(100)-based PCC (blue line in Figure 16 (a)) only one typical peak is detected, that is exactly coincide with the energy (E = 356 meV, λ = 3.48 μm) of band-to-band transition for undoped InAs. Otherwise, the multiple peaks for QDs PCC are detected in both longer and shorter wavelength regions. In particularly, we assume that the shift towards the long wavelengths and the characteristic peaks detected at λ = 3.68 and 3.9 μm are the result of the absorption by the QDs through the

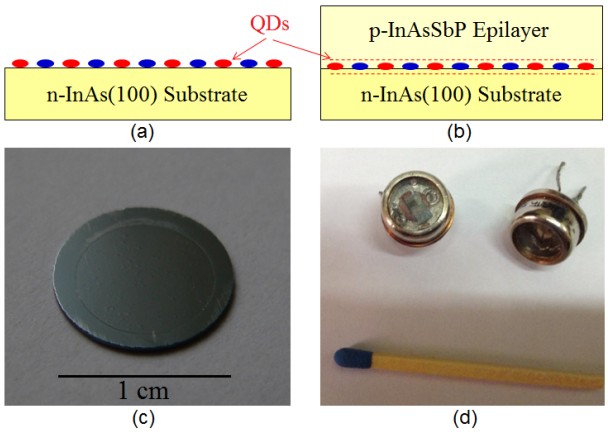

Figure 14: Schematics of In(As,Sb,P)-based mid-infrared QDs PCC and photodiode - (a) and (b); the sample taken from LPE crucible - (c), capsulated (TO-5) mid-IR photodetectors - (d).

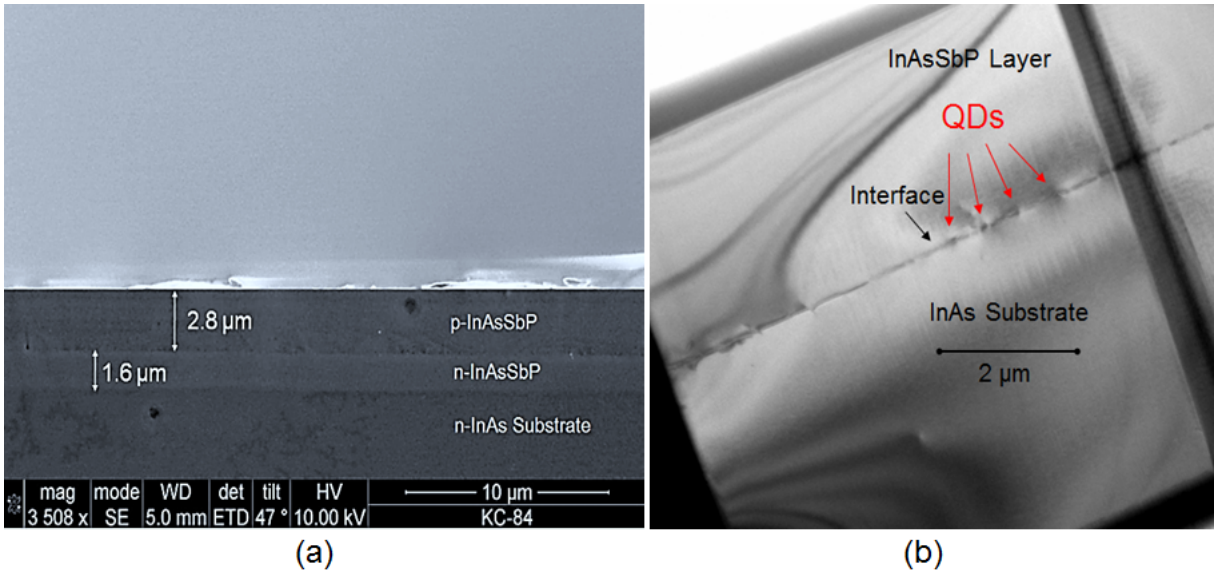

Figure 15: HR-SEM - (a) and TEM - (b) images of In(As,Sb,P)-based QDs mid-infrared diode heterostructures cross sections.

permitted energy sub-band. For Structure 2, an enlargement of the photoresponse spectrum to both longer and shorter wavelength regions is also detected (Figure 16 (b)). Additionally note that in QDs PCC sample the photovoltaic effect has been also detected at zero applied bias. Results of the measurements of the open-circuit voltage (Voc) and short-circuit current (Isc) versus output radiation power density of the He-Ne continuously operated laser at different (λ = 3.39; 1.15 and 0.63 μm) wavelengths are presented in Figure 17. Based on these measurements we calculated the QDs PCC's voltage and current responsivity at room temperature, which are equal to 1.5 V/W and 1 mA/W, respectively at λ = 3.39 μm monochromatic radiation.

For QDs PCC we also performed the same measurements under thermal radiation of the „blackbody" heat source. The room temperature V_{oc} and I_{sc} dependence on distance from the heat source surface (SHS = 1 cm^2) with different temperatures for QDs PCC are presented in Figure 18.

From the experimental results presented in Figures 17 and 17 we conclude that at the incident integral thermal radiation the value of Isc is increased by up to one order compared to that at monochromatic

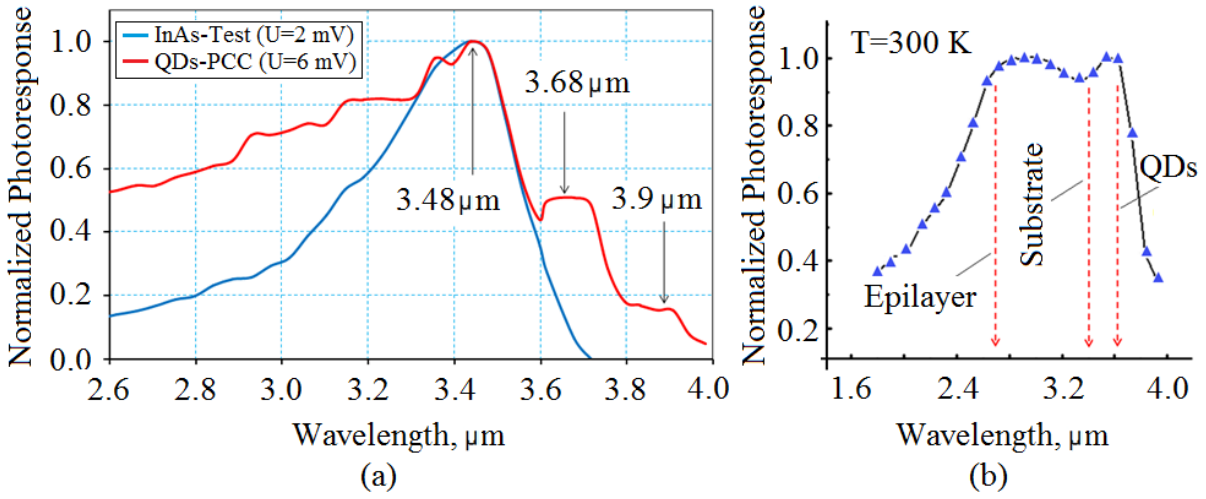

Figure 16: Room temperature normalized photoresponse spectra of In(As,Sb,P)-based QDs PCC - (a) with InAs test sample, and p-In(As,Sb,P)/n-InAs diode heterostructure with QDs embedded into p-n junction spatial charge region - (b).

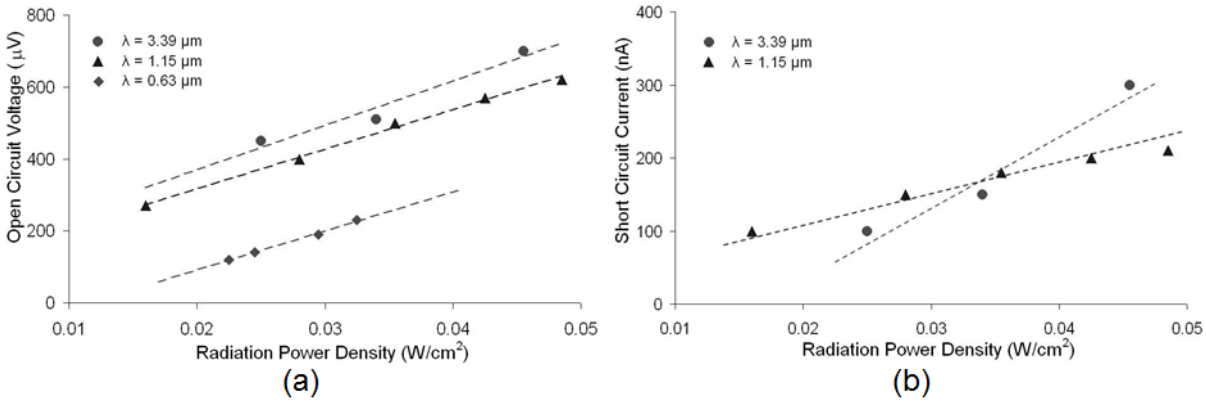

Figure 17: Room temperature open circuit voltage - (a) and short circuit current - (b) of In(As,Sb,P)-based QDs PCC versus radiation power density at different wavelengths of laser irradiation.

radiation. Finally note that in general QDs-based detectors can be expected to exhibit lower dark noise than is present for instance in a quantum well detector. The reduced phonon scattering which results from the discrete density of states in a QD should result in long charge carrier lifetimes and increase the PCC's responsivity and efficiency.

4 Conclusions

In this review paper we have presented results of the growth, characterization and electronic properties of In(As,Sb,P) composition strain-induced micro- and nanostructures. Growth features and the shape transformation of pyramidal islands, lens-shape and ellipsoidal type-II QDs, quantum rings and QD-molecules were described. It was shown that the application of quaternary In(As,Sb,P) composition wetting layer allows not only more flexible monitoring of lattice-mismatch between the wetting layer and an InAs(100) substrate, but also opens up new possibilities at nanoscale engineering and nanoarchitecture of several type of nanostructures. Using an eight-band $\mathbf{k} \cdot \mathbf{p}$ model taking strain and

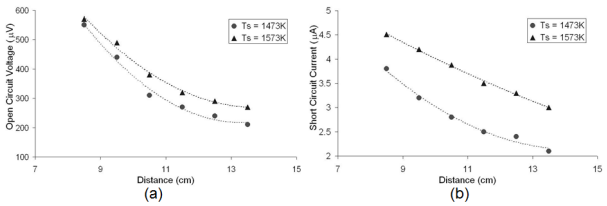

Figure 18: Open circuit voltage - (a) and short circuit current - (b) of In(As,Sb,P)-based QDs PCC versus distance at different temperatures of heat source (S_{HS} = 1 cm^2, $S_{QDs-PCC}$ = 10^{-2} cm^2).

built-in electrostatic potentials into account, the hole ground-state energies and charge densities for a wide range of $InAs_{1xy}Sb_xP_y$ QDs and QD-molecules were computed and the agreement to experimental data identifies this modelling as an ideal tool for theory-guided design of such nanostructures. Two types of QDs mid-infrared photodetectors were fabricated and investigated. It was shown that application of QDs allows to improve relevant output device characteristics, as the sensitivity or the spectral range.

5 Acknowledgment

K.M.G acknowledges funding by the Deutscher Akademischer Austauschdienst (DAAD, German Academic Exchange Service) (Personal ref. no.: 91567213) and State Committee of Science of RA for financial support under grant 18T-2J016. O.M. was funded by the Deutsche Forschungsgemeinschaft (DFG, German Research Foundation) under Germany's Excellence Strategy - EXC2046: MATH+ Berlin Mathematics Research Center (project AA2-5).

References

[1] Y. Aharonov and D. Bohm. Significance of electromagnetic potentials in the quantum theory. *Phys. Rev.*, 115:485–491, Aug 1959.

[2] V. Aroutiounian, K. Gambaryan, and P. Soukiassian. Competing nucleation mechanisms and growth of InAsSbP quantum dots and nano-pits on the InAs(100) surface. *Surface Science*, 604(13):1127 – 1134, 2010.

[3] V. Aroutiounian, S. Petrosyan, A. Khachatryan, and K. Touryan. Quantum dot solar cells. *Journal of Applied Physics*, 89(4):2268–2271, 2001.

[4] T. B. Bahder. Erratum: Eight-band $\mathbf{k} \cdot \mathbf{p}$ model of strained zinc-blende crystals [Phys. Rev. B 41, 11 992 (1990)]. *Phys. Rev. B*, 46:9913–9913, Oct 1992.

[5] P. Bhattacharya, X. H. Su, S. Chakrabarti, G. Ariyawansa, and A. G. U. Perera. *Applied Physics Letters*, 86(19):191106, 2005.

[6] D. Bimberg, M. Grundmann, and N. Ledentsov. *Quantum Dot Heterostructures*. Wiley, 1999.

[7] S. Boeck, C. Freysoldt, A. Dick, L. Ismer, and J. Neugebauer. *Computer Phys. Commun.*, 182:543, 2011.

[8] I. Daruka, J. Tersoff, and A.-L. Barabási. Shape transition in growth of strained islands. *Phys. Rev. Lett.*, 82:2753–2756, Mar 1999.

[9] N. K. Dutta, S. G. Napholtz, R. Yen, R. L. Brown, T. M. Shen, N. A. Olsson, and D. C. Craft. Fabrication and performance characteristics of InGaAsP multiquantum well double channel planar buried heterostructure lasers. *Applied Physics Letters*, 46(1):19–21, 1985.

[10] V. M. Fomin. *Physics of Quantum Rings*. Springer-Verlag, Berlin, Heidelberg, 2014.

[11] C. Freysoldt. Sphinx repository. *sxrepo.mpie.de*.

[12] K. Gambaryan, V. Aroutiounian, T. Boeck, and M. Schulze. The growth of InAsSbP-based diode heterostructures with quantum dots as a new material for thermophotovoltaic application. *physica status solidi c*, 6(6):1456–1459.

[13] K. Gambaryan, V. Aroutiounian, and V. Harutyunyan. Photovoltaic and optoelectronic properties of InAs(100)-based photoconductive cells with quantum dots and nanopits. *Infrared Physics & Technology*, 54(2):114 – 120, 2011.

[14] K. M. Gambaryan. *Nanoscale Res. Lett.*, 5:587, 2010.

[15] K. M. Gambaryan, V. M. Aroutiounian, T. Boeck, M. Schulze, and P. Soukiassian. Strain-induced InAsSbP islands and quantum dots grown by liquid phase epitaxy on a InAs(100) substrate. *Journal of Physics D: Applied Physics*, 41(16):162004, jul 2008.

[16] K. M. Gambaryan, V. M. Aroutiounian, and V. G. Harutyunyan. *Applied Physics Letters*, 101(9):093103, 2012.

[17] K. M. Gambaryan, V. M. Aroutiounian, V. G. Harutyunyan, O. Marquardt, and P. G. Soukiassian. *Applied Physics Letters*, 100(3):033104, 2012.

[18] K. M. Gambaryan, T. Boeck, A. Trampert, and O. Marquardt. Nucleation chronology and electronic properties of $InAs_{1-x-y}Sb_xP_y$ graded composition quantum dots grown on an InAs(100) substrate. *ACS Applied Electronic Materials*, 2(3):646–650, 2020.

[19] K. M. Gambaryan, V. G. Harutyunyan, V. M. Aroutiounian, Y. Ai, E. Ashalley, and Z. M. Wang. *Journal of Physics D: Applied Physics*, 48(27):275302, 2015.

[20] D. Garbuzov, E. Zhuravkevich, A. Zhmakin, Y. Makarov, and A. Ovchinnikov. On the peculiarities of the short-time (tg < 10 ms) solid solution LPE growth onto the moving substrate. *Journal of Crystal Growth*, 110(4):955 – 959, 1991.

[21] A. O. Govorov, S. E. Ulloa, K. Karrai, and R. J. Warburton. Polarized excitons in nanorings and the optical aharonov-bohm effect. *Phys. Rev. B*, 66:081309, Aug 2002.

[22] J. He, C. J. Reyner, B. L. Liang, K. Nunna, D. L. Huffaker, N. Pavarelli, K. Gradkowski, T. J. Ochalski, G. Huyet, V. G. Dorogan, Y. I. Mazur, and G. J. Salamo. Band alignment tailoring of $InAs_{1x}Sb_x$/GaAs quantum dots: Control of type i to type ii transition. *Nano Letters*, 10(8):3052–3056, 2010. PMID: 20698619.

[23] H. Ishikuro and T. Hiramoto. Quantum mechanical effects in the silicon quantum dot in a single-electron transistor. *Applied Physics Letters*, 71(25):3691–3693, 1997.

[24] Y.-F. Lao, S. Wolde, A. G. Unil Perera, Y. H. Zhang, T. M. Wang, H. C. Liu, J. O. Kim, T. Schuler-Sandy, Z.-B. Tian, and S. S. Krishna. InAs/GaAs p-type quantum dot infrared photodetector with higher efficiency. *Applied Physics Letters*, 103(24):241115, 2013.

[25] I. M. Lifshits and V. V. Slezov. Diffusion-controlled decomposition kinetics of supersaturated solid solutions. *Zh. Eksp. Teor. Fiz*, 35(2):8, 1958.

[26] N. Liu, J. Tersoff, O. Baklenov, A. L. Holmes, and C. K. Shih. Nonuniform composition profile in $In_{0.5}Ga_{0.5}As$ alloy quantum dots. *Phys. Rev. Lett.*, 84:334–337, Jan 2000.

[27] O. Marquardt, S. Boeck, C. Freysoldt, T. Hickel, S. Schulz, J. Neugebauer, and E. P. O'Reilly. *Comp. Mat. Sci.*, 95:280, 2014.

[28] O. Marquardt, T. Hickel, J. Neugebauer, K. M. Gambaryan, and V. M. Aroutiounian. *Journal of Applied Physics*, 110(4):043708, 2011.

[29] P. Martyniuk and A. Rogalski. Quantum-dot infrared photodetectors: Status and outlook. *Progress in Quantum Electronics*, 32(3):89 – 120, 2008.

[30] W. Ostwald. Über die vermeintliche Isomerie des roten und gelben Quecksilberoxyds und die Oberflächenspannung fester Körper. *Zeitschrift für Physikalische Chemie*, 34U(1):495 – 503, 1900.

[31] J. Phillips. Evaluation of the fundamental properties of quantum dot infrared detectors. *Journal of Applied Physics*, 91(7):4590–4594, 2002.

[32] E. A. Rezek, N. Holonyak, and B. K. Fuller. Temperature dependence of threshold current for coupled multiple quantum-well $In_{1-x}Ga_x$ $P_{1-z}As_z$-InP heterostructure laser diodes. *Journal of Applied Physics*, 51(5):2402–2405, 1980.

[33] E. Ribeiro, A. O. Govorov, W. Carvalho, and G. Medeiros-Ribeiro. Aharonov-Bohm Signature for Neutral Polarized Excitons in Type-II Quantum Dot Ensembles. *Phys. Rev. Lett.*, 92:126402, Mar 2004.

[34] A. Rogalski. *Acta Phys. Pol. A*, 116:389, 2009.

[35] F. M. Ross, J. Tersoff, and R. M. Tromp. Coarsening of self-assembled Ge quantum dots on Si(001). *Phys. Rev. Lett.*, 80:984–987, Feb 1998.

[36] A. M. Rudin, L. J. Guo, L. I. Glazman, and S. Y. Chou. Charge-ring model for the charge-induced confinement enhancement in stacked quantum-dot transistors. *Applied Physics Letters*, 73(23):3429–3431, 1998.

[37] V. Ryzhii. The theory of quantum-dot infrared phototransistors. *Semiconductor Science and Technology*, 11(5):759–765, may 1996.

[38] I. Stranski and L. Krastanow. *Math. Naturwiss.*, 146:797, 1938.

[39] J. Tersoff and F. K. LeGoues. Competing relaxation mechanisms in strained layers. *Phys. Rev. Lett.*, 72:3570–3573, May 1994.

[40] J. Tersoff, B. J. Spencer, A. Rastelli, and H. von Känel. Barrierless formation and faceting of SiGe islands on Si(001). *Phys. Rev. Lett.*, 89:196104, Oct 2002.

[41] Y. Varshni. *Physica*, 34(1):149 – 154, 1967.

[42] I. Vurgaftman, J. R. Meyer, and L. R. Ram-Mohan. *J. Appl. Phys.*, 89:5815, 2001.

[43] C. Wagner. Theorie der Alterung von Niederschlägen durch Umlösen (Ostwald-Reifung). *Zeitschrift für Elektrochemie, Berichte der Bunsengesellschaft für physikalische Chemie*, 65(7-8):581–591, 1961.

[44] M. Zinke-Allmang, L. C. Feldman, and M. H. Grabow. Clustering on surfaces. *Surface Science Reports*, 16(8):377 – 463, 1992.